Self-Assembled Porphyrin Nanoparticles Interaction Analysis with Albumin by Dynamic Light Scattering

Aleksey R. Krot*, Aleksander I. Ladynin, and Irina A. Sergeeva
Lomonosov Moscow State University, GSP-1, 1–2 Leninskie Gory, Moscow 119991, Russian Federation
*e-mail: ar.krot@physics.msu.ru

Abstract. We herein introduce the study of self-assembled porphyrazine nanoparticles photosensitizers in aqueous solutions with and without a polyvinylpyrrolidone carrier, respectively. For the first time, distributions of hydrodynamic radii for each of the samples separately were obtained, as well as corresponding changes in distributions for multicomponent systems in the presence of human serum albumin. For reliable interpretation of the obtained distributions, a statistical processing method adapted to biological samples was used. The study identified combinations of photosensitizer nanoparticles that could either efficiently interact with human transport proteins or, conversely, maintain their stability in their presence. Thus, the research conducted via dynamic light scattering revealed the potential for fundamentally different passive delivery methods of these nanoparticles: both with and without interaction with the main transport protein of human blood.

Keywords: dynamic light scattering; hydrodynamic radius; photodynamic therapy; self-assembled photosensitizers; porphyrazines; human serum albumin.

Paper #9058 received 14 Jan 2024; revised manuscript received 22 Apr 2024; accepted for publication 1 May 2024; published online 28 May 2024. doi: 10.18287/JBPE24.10.020305.

1 Introduction

According to current data from the World Health Organization, about 9.3 million deaths from cancer were recorded in 2019. Malignant neoplasms are the second leading cause of death after cardiovascular diseases [1]. Cancer is one of the most important problems of the modern world. Among the treatment concepts for cancer, photodynamic therapy (PDT) can be highlighted − a modern, organ-preserving treatment method used in medicine. PDT is a local method for the treatment of various cancers, in which an intravenously administered photoactive drug, a photosensitizer (PS), accumulates in the tumor tissue in a higher concentration than in the surrounding tissues, and is activated after irradiation with light with a wavelength corresponding to its long-wave absorption peak. The photodynamic reaction that occurs in the presence of tissue oxygen causes the generation of singlet oxygen, which leads to tumor cells damage. The effect of reactive oxygen species is manifested by direct cytotoxic damage to malignant cells and destruction of blood vessels feeding the tumor. PS can also be used to diagnose cancer [2].

The process of delivering PS nanoparticles to tumor tissues is carried out by intravenous injection into the bloodstream, and currently two fundamental approaches can be distinguished that explain the effective passive targeting of nanoparticles:

1. Enhanced Permeability and Retention (EPR) effect which is still an active area of research and also a subject of debate [3, 4];

2. Methods based on the binding of human serum albumin (HSA), a transport protein, with PS particles [5−7].

In the first case, to realize the EPR effect, it is necessary to maintain the stability of the PS in the bloodstream, ideally obtaining nanoparticles of a deterministic size with a complete absence of interaction in the bloodstream. Under such conditions, the effect of targeted delivery to tumor tissues is expected to be maximized.

The second scenario represents a fundamentally diametrical concept in which, upon intravenous administration, the PS binds to blood proteins, leaving only a minor portion in a free state. Dye molecules attach to proteins due to electrostatic, hydrophobic, and

This paper was presented at the Annual International Conference Saratov Fall Meeting XXVII, Saratov, Russia, September 25–29, 2023.

hydrogen interactions, as well as van der Waals forces. For instance, a single low-density lipoprotein molecule is capable of transporting up to 1000 molecules of a hydrophobic photosensitizer [8]. Tetraphenylporphines are mainly transported by albumin, while chlorin is bound approximately to the same extent to high-density lipoproteins and albumin [9].

The search for successful compounds that act as building blocks for PS is a subject of increased interest in the field of photodynamic therapy. The subjects of this study are water-soluble porphyrazine-based PS, capable of independently dissolving into stable nanosized micellar structures under the codenames PT_peg and S_27_Na. These compounds are heterocyclic analogs of magnesium phthalocyanine with reduced A3B-type symmetry [10]. S_27_Na nanoparticles contain a carboxyl group, which determines a number of important properties of the photosensitizer and is widely used in potential pharmacoforms [11, 12]. The polyethylene glycol group in the PT_peg structure additionally has the function of masking the micelle from its interaction with blood proteins, providing increased stability of nano-sized micellar structures in the bloodstream and greatly enhanced the drug-loading ratio of the single polymers [13, 14].

The optical method of Dynamic Light Scattering (DLS) enables the investigation of albumin molecule solutions and PS nanoparticles under conditions approximating the physiological. Using DLS, it is possible to study nanoparticles without altering their structure, making this method a practical standard when working with a such type particles [15−17]. In the study [5], DLS was used to analyze similar zinc phthalocyanine nanoparticles, demonstrating their complete disappearance in the presence of transport proteins due to dissassembling of the PS complexes under modeled conditions. This work is the first to study a set of samples with a wide range of characteristics under passive load conditions, where polyvinylpyrrolidone (PVP) serves as a model drug. The separate binding of PVP to HSA was also demonstrated, which is a characteristic interaction between PVP and transport proteins [18, 19].

2 Experimental Method

To measure the nanoparticles sizes, as well as to monitor the dynamics of changes in the contributions of the molecules solution hydrodynamic radii, the dynamic light scattering method was used. The parameters of the PS dispersed in the liquid were measured using a Photocor Complex particle analyzer. The installation diagram is shown in Fig. 1.

The DLS method is based on the correlation function (CF) analysis of the number of photons over time recorded in a scattering volume in a given direction. The Brownian motion of scattered objects, in this case PS nanoparticles, causes temporary fluctuations in the intensity of scattered light. Thus, by analyzing the received signal, the correlator calculates an autocorrelation function expressing the correlation of the scattered light intensity over time τ:

$$G(\tau) = \langle I(t)I(t+\tau)\rangle, \quad (1)$$

where averaging is performed over time t:

$$\langle I(t)I(t+\tau)\rangle = \lim_{\Delta t\to\infty}\frac{1}{\Delta t}\int_0^{\Delta t} I(t)I(t+\tau)dt \ , \quad (2)$$

where Δt is the accumulation time of correlation function. In this case, according with Onsager's hypothesis the relaxation of local concentration fluctuations is described by the diffusion Eq.:

$$\frac{\partial c(\boldsymbol{r},t)}{\partial t} = -D\nabla c(\boldsymbol{r},t), \quad (3)$$

where $c(\boldsymbol{r},t)$ – concentration, D – particle diffusion coefficient. Generally, DLS instruments export the normalized version of $G(\tau)$:

$$g^{(2)}(\tau) = \frac{<I(t)I(t+\tau)>}{<I(t)>^2}. \quad (4)$$

The normalized second-order autocorrelation function $g^{(2)}(\tau)$ can be related to the normalized first-order correlation function $g^{(1)}(\tau)$ through the Siegert Eq. [20]:

$$g^2(\tau) = 1 + \beta[g^{(1)}(\tau)]^2, \quad (5)$$

where the first term of the sum is related to the baseline value (≈1) and the parameter β is the coherence factor that depends on the instrument and the scattering properties of macromolecules.

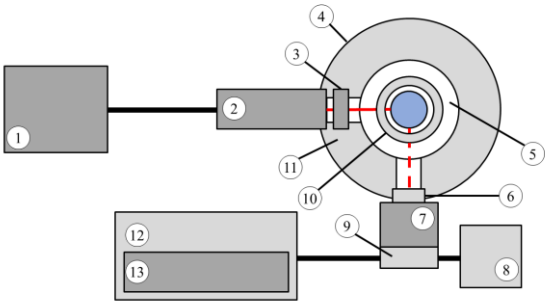

Fig. 1 Photocor Complex experimental setup schematic diagram: 1 − power supply, 2 − laser (445 nm or 647 nm), 3 − focusing lens, 4 − cuvette adapter, installed coaxially with the axis of the goniometer, 5 − goniometer console, 6 − receiving optical system (at 90°), 7 − photomultiplier operating in photon counting mode, 8 − special high-voltage power supply for PMT without parasitic correlations, 9 − amplifier-discriminator with a direct current bypass, 10 − thermostat, 11 − rigid base, 12 − personal computer, 13 − correlator directly connected to the personal computer.

The function $g^{(1)}(\tau)$ contains information about the movement of particles and for monodisperse particles the system decreases exponentially. In the general case (for polydisperse systems), $g^{(1)}(\tau)$ is an intensity-weighted integral over the distribution of decay rates $G(\Gamma)$:

$$g^{(1)}(\tau) = \int_0^\infty G(\Gamma) e^{(-\Gamma\tau)} d\Gamma, \quad (6)$$

where $G(\Gamma)$ is normalized: $\int_0^\infty G(\Gamma) d\Gamma = 1$, Γ the inverse correlation time:

$$\Gamma = \frac{1}{t_c} = D_t q^2, \quad (7)$$

where the wave vector of concentration fluctuations has the following form:

$$q = \frac{4\pi n}{\lambda} \sin\frac{\theta}{2}, \quad (8)$$

where n is the refractive index of the medium, λ is the wavelength of laser radiation, θ is the scattering angle. Using the Stokes-Einstein relation:

$$D = \frac{k_B T}{6\pi\eta R_h}, \quad (9)$$

where k_B is the Boltzmann constant, T is the absolute temperature of the medium, η is the viscosity coefficient of the medium where particles of radius R_h are suspended. R_h – hydrodynamic or Stokes radius, calculated based on the spherical shape assumption of an object. Thus, based on the approximation of the scattered light intensity autocorrelation function using Eq. (7), it is possible to determine the particle diffusion coefficient and, ultimately, the sizes of the particles under study from the Eq. (9) [21−23].

Results are often processed using software provided by the supplier of the experimental setup, in particular, the DynaLS software program is recommended as the primary data analysis tool for DLS. However, in the case of working with a multicomponent system whose individual component contribution are unknown in advance, this approach can greatly increase subjective error. The need to select specific channel ranges, points of the correlation function for result processing, visual monitoring of residuals − forms of deviation from experimental data to the chosen model, and subjective regulation of the acceptable level of scattering intensity deviation from its average value can lead to significant distortions in the accurate ranges of the system's average hydrodynamic radius.

In order to avoid such errors, this work used a statistical method of data processing, a modified approach used in Raynals − software for analyzing DLS data using Tikhonov-Phillips regularization [24]. The main advantages of this approach are the uniformity of processing rules, as well as the working speed with large data. The final distribution was analyzed based on the results of averaging all measurements, which made it possible to level out noise in the data and random deviations from the true size components contributions, simultaneously without the use of special corrective rules that could distort the true values.

3 Results and Discussions

Samples of PS nanoparticles (PT_peg and S_27_Na) were studied separately and using the synthetic polymer polyvinylpyrrolidone (PVP), which in this case acted as a passive load. In the future, therapeutic agents already known in medical practice, such as doxorubicin, could replace PVP as the payload. The interaction study of PS nanoparticles with the main transport protein of human blood HSA was conducted using 20% (200 g/L) albumin from "Octapharma" [25].

To resolve two peaks in the hydrodynamic radii distribution, their radius must differ by at least two times. Thus, the interaction between albumin and PS can be detected if a new stable and distinguishable peak appears with a size different from the peaks of HSA and PS.

During data processing, two main analysis approaches were identified. The empirical approach involves a sequential analysis of each measurement in the DynaLS program, based on the results of preliminary processing of all correlation functions obtained for the corresponding concentrations of the substance in an aqueous solution. In such cases, the dependence of the nanoparticles hydrodynamic radius reaches a plateau when concentrations are reached that are sufficient to exceed the contribution of the instrumental error − the phenomenon of an artifact peak [26]. To minimize subjective corrections, the following methods of averaging accumulated data were considered, taking into account the contributions of correlation functions individual components (Fig. 2):

1. distribution function for peaks of maximum contributions of averaged autocorrelation functions (Fig. 2a, b);
2. distribution function for all maxima of radius distributions (Fig. 2(c, d));
3. distribution function for all conducted measurements (Fig. 2(e)).

The most reliable and closest to the empirical approach was found to be the third method of averaging (Fig. 2(e)), which was chosen as the main approach for analyzing scattering data. To calculate the averaged radius distribution function, between 20 to 30 separate distribution functions were averaged. Similarly, the results about the sizes of the sample with PVP, as well as the sizes of nanoparticles S_27_Na and S_27_Na_PVP, were obtained (Fig. 3). Fig. 3 shows the corresponding graphs depicting the dependence of scattered light intensity on concentration during the measurements, which should have a linear dependence in accordance with Rayleigh's law:

$$I \sim n, \quad (10)$$

where I – scattered light intensity, n – number of particles per unit volume.

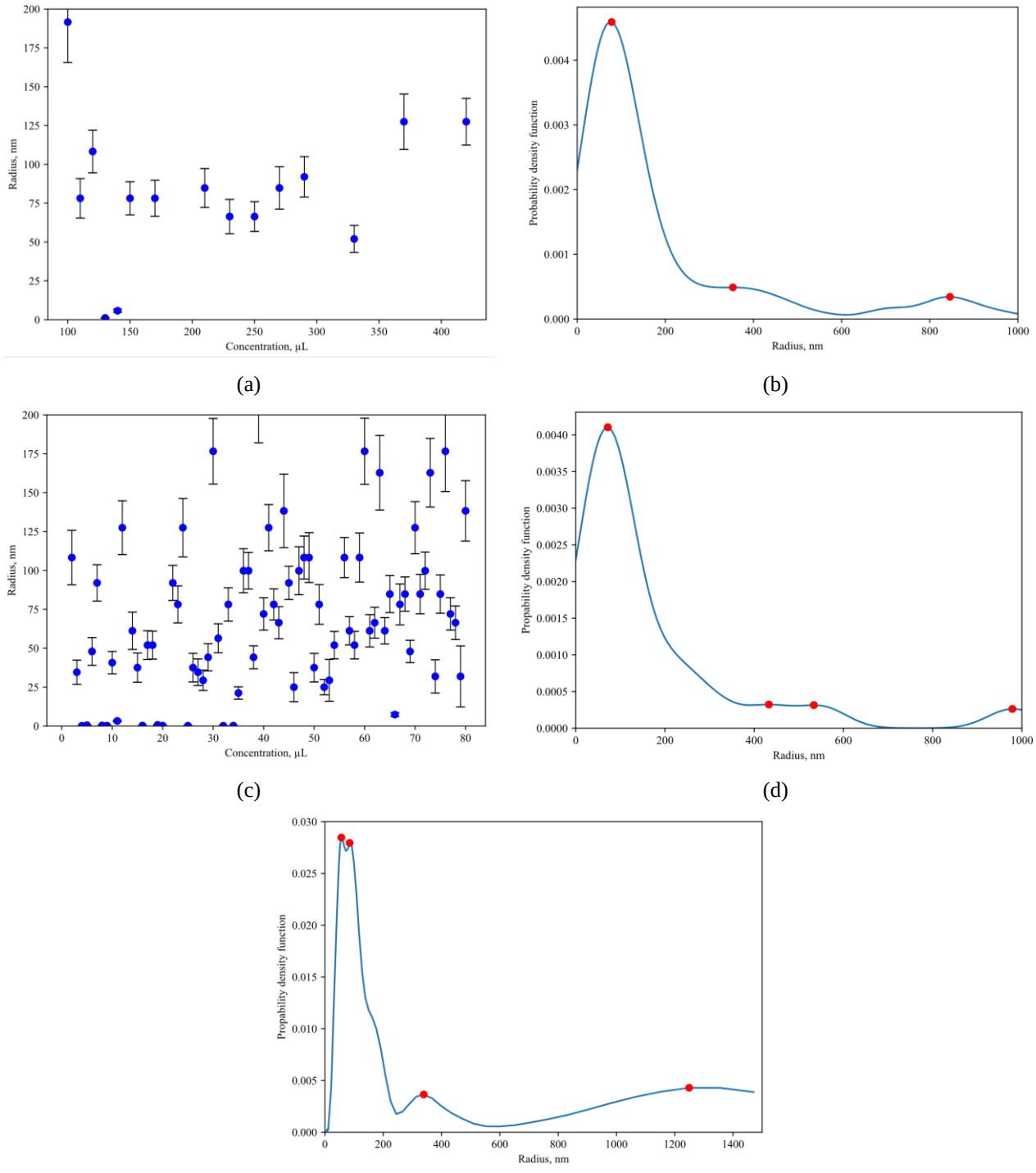

Fig. 2 Comparative analysis of averaging techniques: (a) all peaks of the radius distribution against the concentration of PS PT_peg. (b) Probability density function for the corresponding size of PS PT_peg across all peaks. (c) All peaks of the radius distribution by experiment number for PS PT_peg. (d) Probability density function for the corresponding size of PS PT_peg for averaged CFs. (e) Averaged probability density function for the corresponding size of PS PT_peg across all measurements.The red dots are the extremum points of the distribution density function.

The result nanoparticles sizes are given in Table 1.

It should also be noted that not all identified peak values are interpreted as the complexes sizes of the corresponding photosensitizer. For example, the last peak with order values of 1 μm and higher is an artifact peak that is not a real value and arises as a result of working with highly diluted solutions. Fig. 3(d) shows a peak of several nanometers, representing free PVP particles.

Similarly, the HSA sizes components were measured. Fig. 4 shows the mean hydrodynamic radius distribution of HSA in aqueous solution as a function of concentration, as well as the intensity of scattered light.

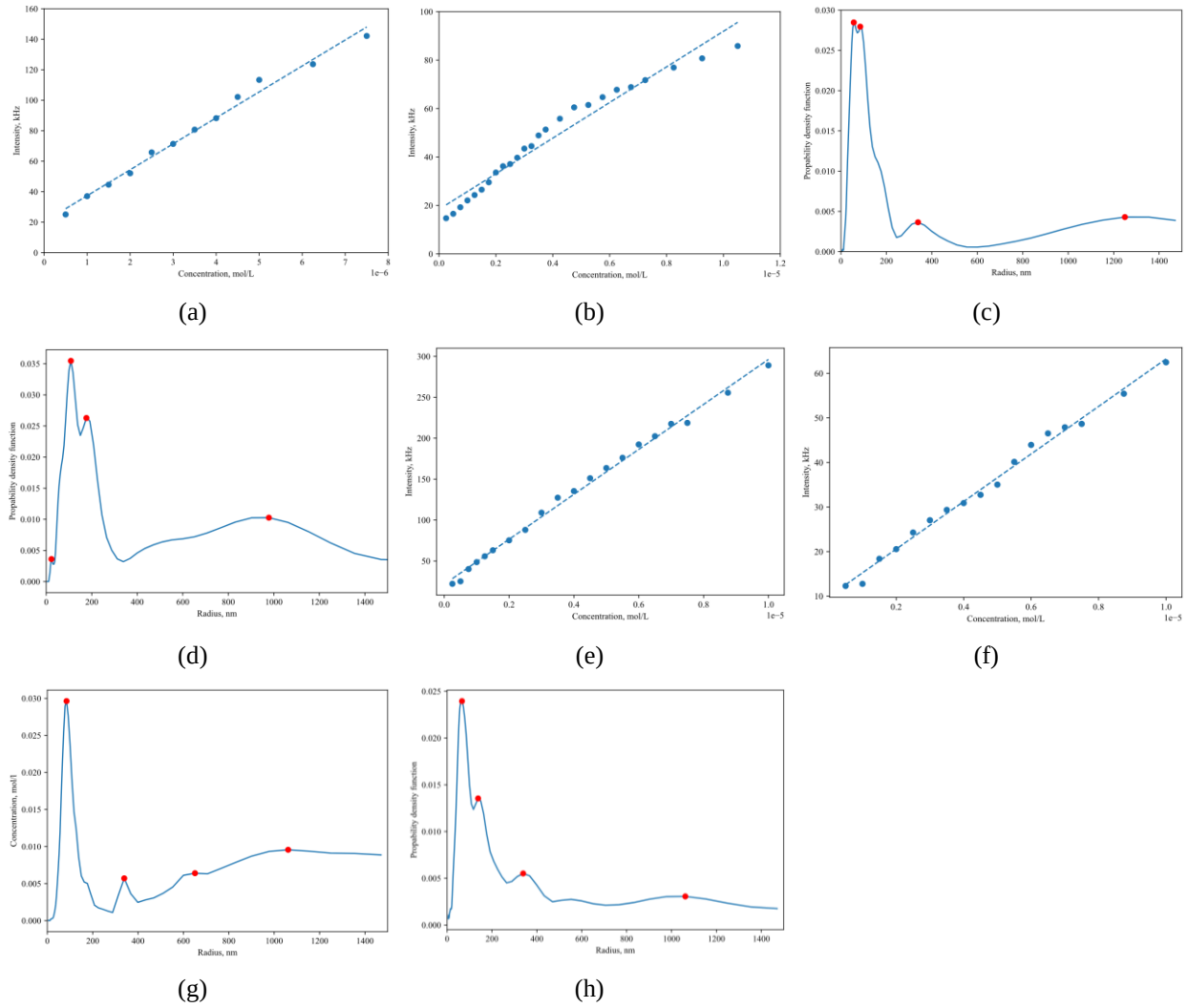

Fig. 3 Hydrodynamic radius determination for all samples: (a) Intensity vs. concentration of PT_peg. (b) Intensity vs. concentration of PT_peg_PVP. (c) Probability densities for the corresponding size of PS PT_peg. (d) Probability densities for the corresponding size of PS PT_peg_PVP. (e) Intensity vs. concentration of S_27_Na. (f) Intensity vs. concentration of S_27_Na_PVP. (g) Probability densities for the corresponding size of PS S_27_Na. (h) Probability densities for the corresponding size of PS S_27_Na_PVP. The red dots are the extremum points of the distribution density function. Blue dots − scattered light intensity for relevant concentrations. Dotted line − linear regression.

Table 1 Hydrodynamic radii values of PS nanoparticles.

Sample	Hydrodynamic radius, nm
PT_peg	45 ± 14 112 ± 37
PT_peg_PVP	90 ± 28 197 ± 40
S_27_Na	92 ± 38 336 ± 24
S_27_Na_PVP	62 ± 23 162 ± 36 339 ± 52

Thus, the sizes of HSA in aqueous solution at pH ~ 7.5 are 3.6 ± 0.9 nm and 36 ± 10 nm respectively, where the first size corresponds to the literature data, and the second represents an energetically favorable aggregate of protein molecules.

Thus, having reliably determined the individual sizes contributions of nanoparticles and HSA separately, it is possible to draw conclusions about the presence or absence of a characteristic interaction through a similar analysis of HSA with the corresponding photosensitizer in an aqueous solution, having previously selected the concentrations so that the intensity contribution of the components is comparable and does not overlap the contributions individual particles. Table 2 presents the concentration ranges of the samples that were used in this study.

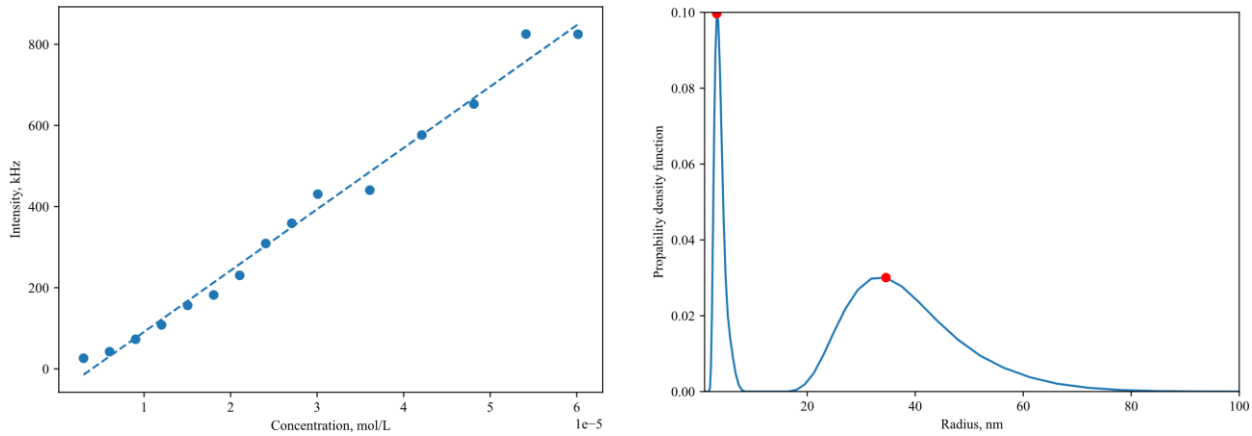

(a) (b)

Fig. 4 Hydrodynamic radius determination for HSA: (a) Intensity vs. concentration of HSA. (b) Probability densities for corresponding size of HSA. The red dots are the extremum points of the distribution density function. Blue dots − scattered light intensity for relevant concentrations. Dotted line − linear regression.

Table 2 Ranges of samples limit concentrations.

Sample	Minimum concentration, mol/l	Maximum concentration, mol/l	Ranges of sample volumes, μL
PT_peg	$1.25 \cdot 10^{-6}$	$1.5 \cdot 10^{-5}$	50−600
PT_peg_PVP	$1.25 \cdot 10^{-6}$	$1.5 \cdot 10^{-5}$	50−600
S_27_Na	$2.5 \cdot 10^{-6}$	$3 \cdot 10^{-5}$	50−600
S_27_Na_PVP	$2.5 \cdot 10^{-6}$	$3 \cdot 10^{-5}$	50−600
HSA	$1 \cdot 10^{-5}$	$3 \cdot 10^{-5}$	14−40

Let us consider the probability density distribution functions for the hydrodynamic radii in the aqueous solution of PT_peg with HSA and PT_peg_PVP with HSA, respectively, presented in Fig. 5 (a, b). With a fixed concentration of HSA ($n = 3 \times 10^{-5}$ mol/L), the concentration of PS nanoparticles was increased, eventually reaching a PS/HSA ratio of 1:2. Fig. 5(c, d) highlights the size distribution functions of the nanoparticles separately for pure HSA, PS, and their solution at the maximum concentration ratio.

Fig. 5(c) shows a repetition of the HSA size distribution peaks in HSA and PT_peg solution, with a slight increase in size. This increase is associated with a decrease in the influence of the artifact peak due to an increase in the total concentration of the solution. The absence of other peaks is due to the overlap of the signal from the sizes of nanoparticles; however, additional sizes are not observed, which indicates the absence protein interaction with the PT_peg sample. Fig. 5(d) shows a similar picture of the size distribution, but in this case a new peak appears that does not correspond to the sizes of either the protein or the PS nanoparticles. However, this size is not the result of the nanoparticles interaction with HSA. In this case, a corresponding peak in the interaction of PT_peg with the HSA would be observed, instead we detect the formation of protein associates with free PVP particles.

A similar distribution is shown for S_27_Na and HSA in Fig. 6, however, in this case, in the absence of PVP as a passive PS load, we see a new peak that does not correspond to either the individual sizes of HSA or S_27_Na, which indicates the interaction of nanoparticles with the main transport protein. In the case of S_27_Na_PVP, such a distribution is not informative, since it is not possible to identify specific peaks. Taking into account the interaction of S_27_Na NPs separately, as well as free PVP with HSA, a picture of multiple intensity contribution peaks was obtained over a large number of sizes, which cannot be resolved individually (Fig. 7(b)). For comparison, Fig. 7(a) shows the corresponding distribution of peaks in the case of individual S_27_Na PVP nanoparticles, where, in the absence of any interactions, repeatable and reproducible peaks are observed with increasing concentration of the substance. The rightmost peak is an artifact peak, which in this case does not represent the real size, but is typical when working with highly dilute solutions [26].

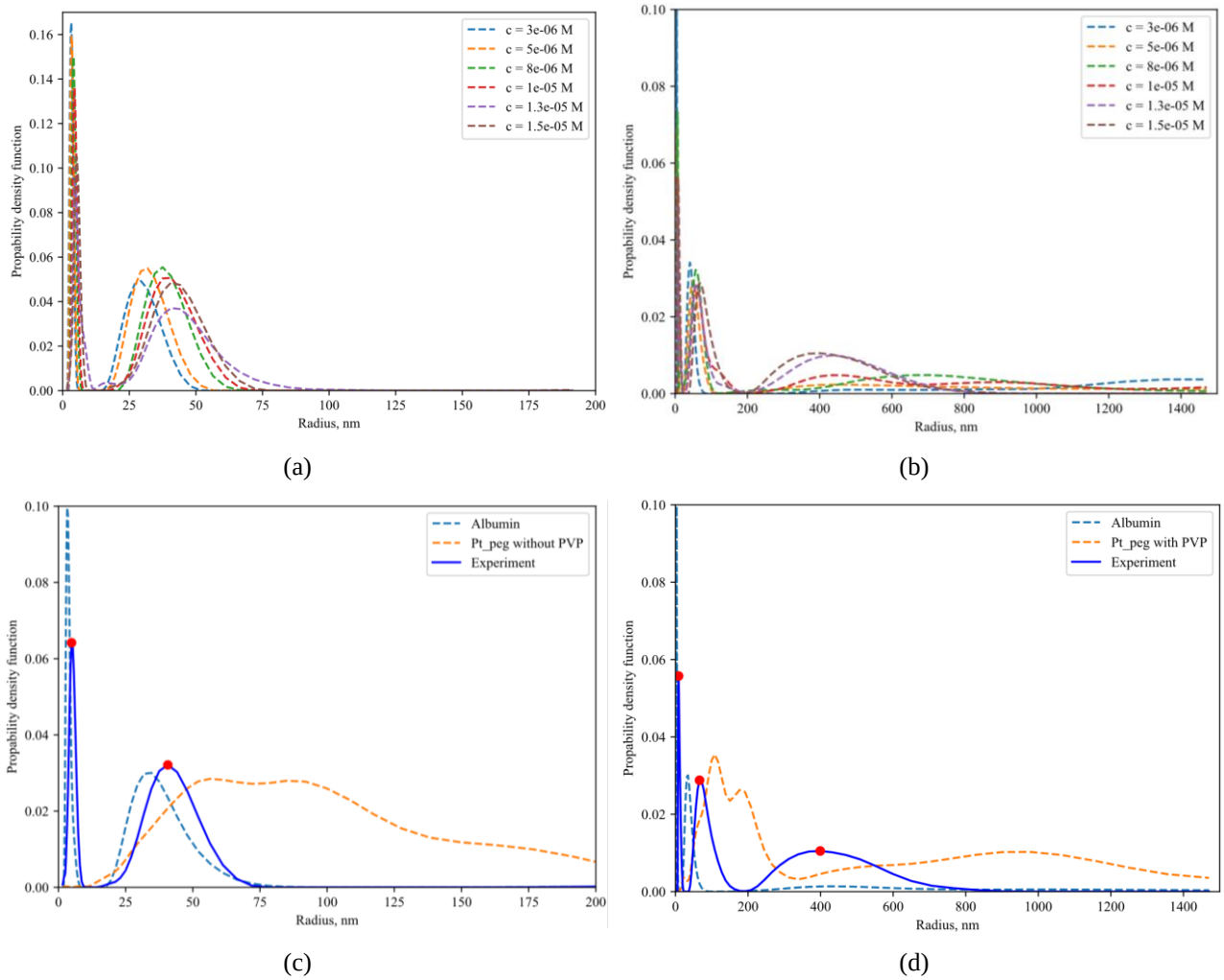

Fig. 5 Hydrodynamic radius determination for PT_peg with HSA: (a) Probability densities for corresponding size of aqueous solution of PT_peg and HSA. (b) Probability densities for corresponding size of aqueous solution of PT_peg_PVP and HSA. The red dots are the extremum points of the distribution density function.

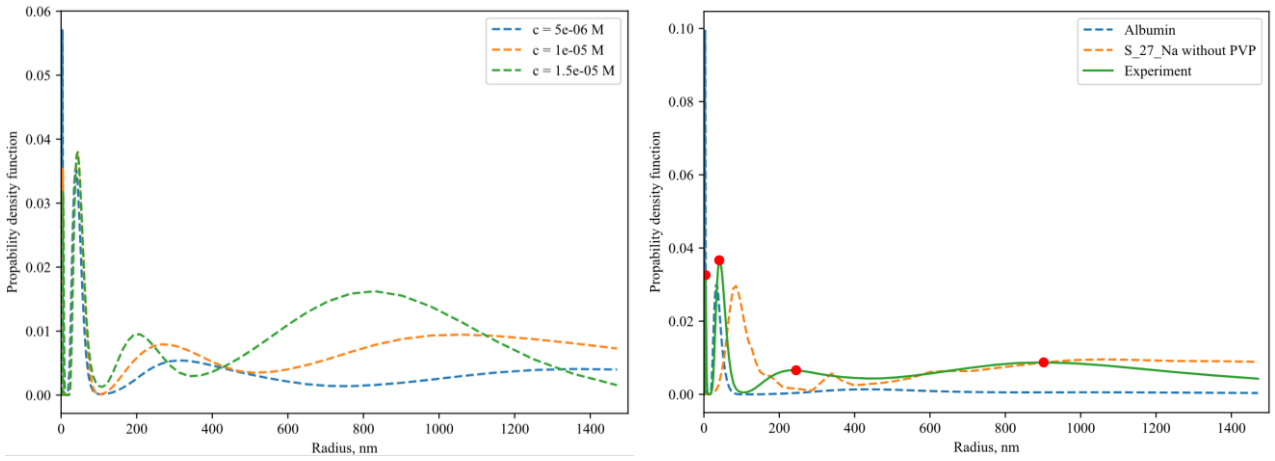

Fig. 6 Hydrodynamic radius determination for S_27_na with HSA: (a) Probability densities for corresponding size of aqueous solution (S_27_Na and HAS). (b) Comparison of probability density functions for corresponding sizes separately for HSA, S_27_Na, and solution. The red dots are the extremum points of the distribution density function.

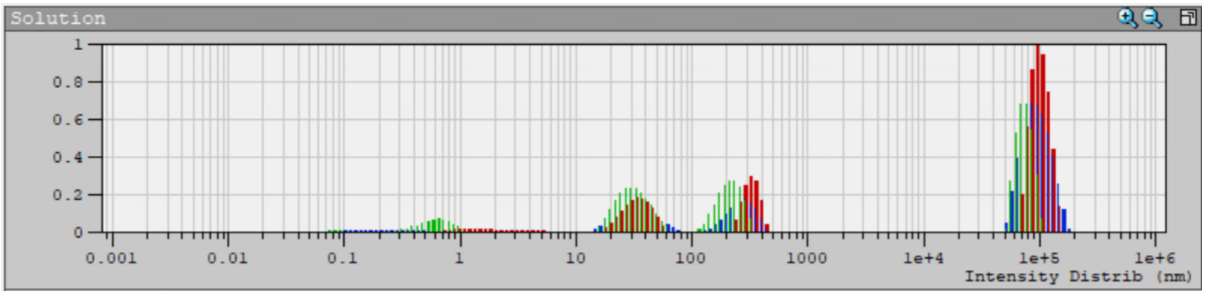

(a)

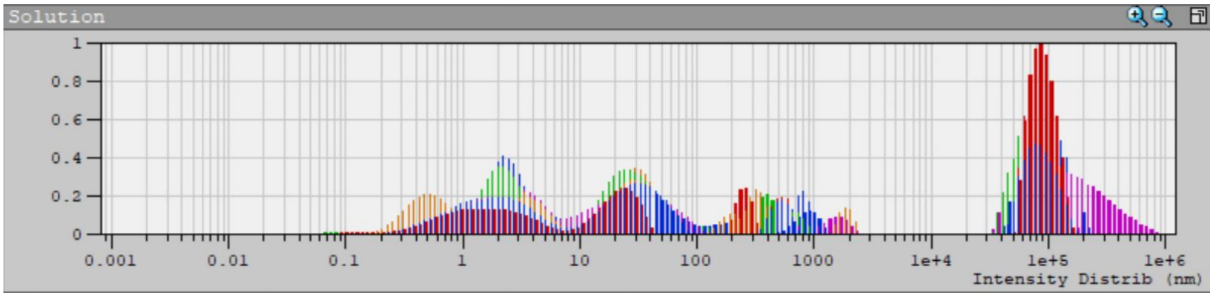

(b)

Fig. 7 (a) Peak distribution for S27_Na with PVP without HAS. DynaLS Software. (b) Peak distribution for S27_Na with PVP with HSA (Photosensitizer/Albumin Ratio = 1:1). DynaLS Software. Colors determine individual accumulations of correlation functions.

Table 3 Summary sample statistics.

Sample	Hydrodynamic radius, nm	Presence of a new peak in solution with albumin	PS interaction with albumin
HSA	3.6 ± 0.9 36 ± 10	–	–
Pt_peg	45 ± 14 112 ± 37	Absence	Absence of interaction
Pt_peg_PVP	90 ± 28 197 ± 40	New peak (400 nm)	Presence of interaction
S27_Na	92 ± 38 336 ± 24	New peak (215 nm)	Presence of interaction
S27_Na_PVP	62 ± 23 162 ± 36 339 ± 52	Multiple new peaks	Presence of interaction

4 Conclusions

In this way, all observed sizes were obtained in the study of aqueous solutions of PS with HSA (Table 3).

The work demonstrated the effectiveness of the statistical approach in data processing when working with multicomponent biological media in comparison with the use of basic software.

It was found that the Pt_peg type sample has the most stable state in the presence of transport HSA, whereas the S27_Na sample tends to interact with the protein.

Additionally, the presence of PVP in the solution promotes a more pronounced interaction of HSA particles with the corresponding NPs.

As a result of a comparative analysis of self-assembled porphyrazine nanoparticles with and without PVP, properties were identified that make it possible to implement various methods of targeted drug delivery to tumor tissues.

The DLS method revealed characteristic patterns in the interaction, or its complete absence, of the studied photosensitizer nanoparticles with HSA. Further research is focused on studying the process kinetics, in particular the binding constants and other parameters of the observed interaction.

Disclosures

The authors declare that they have no conflict of interest.

References

1. "World health statistics 2023: monitoring health for the SDGs, sustainable development goals, " World Health Organization Global report (2023) (accessed 20 April 2024). [https://www.who.int/publications/i/item/9789240074323].
2. E. V. Yaroslavtseva-Isaeva, A. L. Zubarev, V. N. Kapinus, A. A. Kurilchik, V. E. Ivanov, and A. L. Starodubtsev, "Intraoperative photodynamic therapy in the combined treatment of soft tissue sarcoma, " Laser Medicine 26(3–4), 9–15 (2022) [in Russian].
3. R. Sun, J. Xiang, Q. Zhou, Y. Piao, J. Tang, S. Shao, Z. Zhou, Y. H. Bae, and Y. Shen, "The tumor EPR effect for cancer drug delivery: Current status, limitations, and alternatives," Advanced Drug Delivery Reviews 191, 114614 (2022).
4. M. Ikeda-Imafuku, L. L. W. Wang, D. Rodrigues, S. Shaha, Z. Zhao, and S. Mitragotri, "Strategies to improve the EPR effect: A mechanistic perspective and clinical translation," Journal of Controlled Release 345, 512–536 (2022).
5. X. Li, S. Yu, Y. Lee, T. Guo, N. Kwon, D. Lee, S. C. Yeom, Y. Cho, G. Kim, J.-D. Huang, S. Choi, K. T. Nam, and J. Yoon, "In vivo albumin traps photosensitizer monomers from self-assembled phthalocyanine nanovesicles: a facile and switchable theranostic approach," Journal of the American Chemical Society 141(3), 1366–1372 (2019).
6. A. Costa-Tuna, O. A. Chaves, R. J. S. Loureiro, S. Pinto, J. Pina, and C. Serpa, "Interaction between a water-soluble anionic porphyrin and human serum albumin unexpectedly stimulates the aggregation of the photosensitizer at the surface of the albumin," International Journal of Biological Macromolecules 255, 128210 (2024).
7. Y. Li, D. Zhang, Y. Yu, L. Zhang, L. Li, L. Shi, G. Feng, and B. Z. Tang, "A Cascade Strategy Boosting Hydroxyl Radical Generation with Aggregation-Induced Emission Photosensitizers-Albumin Complex for Photodynamic Therapy," American Chemical Society 17, 16993–17003 (2023).
8. W. M. Sharman, J. E. van Lier, and C. M. Allen, "Targeted photodynamic therapy via receptor mediated delivery systems," Advanced Drug Delivery Reviews 56(1), 53–76 (2004).
9. A. S. Sobolev, D. A. Jans, and A. A. Rosenkranz, "Targeted intracellular delivery of photosensitizers," Progress in Biophysics and Molecular Biology 73(1), 51–90 (2000).
10. P. A. Tarakanov, M. E. Neganova, D. V. Mishchenko, S. D. Bondarenko, I. A. Sergeeva, A. R. Krot, N. S. Goryachev, A. O. Simakov, M. S. Kukharsky, S. A. Pukhov, and V. E. Pushkarev, "Low-symmetry A3 B-type 6H-1,4-diazepinoporphyrazines with anti-Kasha effect as promising photosensitizers," Photochemistry and Photobiology (2024).
11. Q. Zhang, J. He, W. Yu, Y. Li, Z. Liu, B. Zhou, and Y. Liu, "A promising anticancer drug: a photosensitizer based on the porphyrin skeleton," RSC Medicinal Chemistry 11(4), 427–437 (2020).
12. G. B. Bodedla, W. Y. Wong, and X. Zhu, "A couple of new porphyrin photosensitizer and cobaloxime cocatalyst for highly efficient photocatalytic H2 evolution," Journal of Materials Chemistry A 9(36), 20645–20652 (2021).
13. B. Xiang, Y. Xue, Z. Liu, J. Tian, H. Frey, Y. Gao, and W. Zhang, "Water-soluble hyperbranched polyglycerol photosensitizer for enhanced photodynamic therapy," Polymer Chemistry 11(23), 3913–3921 (2020).
14. N. Plekhova, O. Shevchenko, O. Korshunova, A. Stepanyugina, I. Tananaev, and V. Apanasevich, "Development of Novel Tetrapyrrole Structure Photosensitizers for Cancer Photodynamic Therapy," Bioengineering 9(2), 82 (2022).
15. Y. Takano, E. Hirata, N. Ushijima, H. Harashima, and Y. Yamada "An effective in vivo mitochondria-targeting nanocarrier combined with a π-extended porphyrin-type photosensitizer," Nanoscale Advances 3(20), 5919–5927 (2021).
16. Y. S. Bortnevskaya, N. A. Shiryaev, N. S. Zakharov, O. O. Kitoroage, M. A. Gradova, N. Y. Karpechenko, A. S. Novikov, E. D. Nikolskaya, M. R. Mollaeva, N. G. Yabbarov, N. A. Bragina, and K. A. Zhdanova, "Synthesis and biological properties of egfr-targeted photosensitizer based on cationic porphyrin," Pharmaceutics 15(4), 1284 (2023).
17. S. Kirar, D. Chaudhari, N. S. Thakur, S. Jain, J. Bhaumik, J. K. Laha, and U. C. Banerjee, "Light-assisted anticancer photodynamic therapy using porphyrin-doped nanoencapsulates," Journal of Photochemistry and Photobiology B: Biology 220, 1011–1344 (2021).
18. S. Hashemnia, H. Zarei, Z. Mokhtari, and M. H. Mokhtari, "An investigation of the effect of PVP-coated silver nanoparticles on the interaction between clonazepam and bovine serum albumin based on molecular dynamics simulations and molecular docking," Journal of Molecular Liquids 323, 114915 (2021).
19. S. B. Suryawanshi, N. K. Desai, A. J. Bodake, and S. R. Patil, "Fluorescence Enhancement Based Quantification of Human Serum Albumin from Biological Sample Using Indole Based Nanosuspension: Molecular Interactions and Molecular Docking Studies," Journal of Fluorescence 32, 293–305 (2022).
20. A. J. F. Siegert, Dynamic on the fluctuations in signals returned by many independently moving scatterers, Radiation laboratory, Massachusetts Insitute of Technology (1943).
21. L. V. Levshin, A. M. Saletsky, Optical methods for studying molecular systems, Moscow State University Publishing, Moscow House (1994). [in Russian].
22. H. Z. Cummins, E. R. Pike (Eds.), Photon Correlation and Light Beating Spectroscopy, Springer Science, New York, (1974). ISBN: 9781461589068.

23. R. Pecora, Dynamic Light Scattering, Plenum Press, New York (1985).
24. O. Burastero, G. Draper-Barr, B. Raynal, M. Chevreuil, P. England, and M. G. Alai, "Raynals, an online tool for the analysis of dynamic light scattering," Acta Crystallographica Section D: Structural Biology 79(8), 673–683 (2023).
25. "Human serum albumin," Octapharma (accessed 24 April 2024). [https://www.octapharma.com/products/industrial-collaboration/human-serum-albumin].
26. M. N. Kirichenko, A. T. Sanoeva, and L. L. Chaikov, "The appearance of an artifact peak in the particle size distribution measured by the DLS method at low concentrations," Brief Communications on Physics of the Physical Institute Named after P. N. Lebedev Russian Academy of Sciences 43(8), 32–38 (2016). [in Russian].